PHYSICAL REVIEW A VOLUME 44, NUMBER 10 15 NOVEMBER 1991

Scale-invariant regimes in one-dimensional models of growing and coalescing droplets

B. Derrida
Service de Physique Théorique, Commissariat à l'Energie Atomique, Saclay, 91191 Gif-sur-Yvette CEDEX, France

C. Godrèche and I. Yekutieli
Service de Physique du Solide et de Résonance Magnétique, Commissariat à l'Energie Atomique, Saclay, 91191 Gif-sur-Yvette CEDEX, France

(Received 4 March 1991)

We consider several simplified models of breath figures in one dimension. For all these models, the combined effects of growth and of coalescence of droplets lead to a scale-invariant regime with a stable distribution of the distances between droplets. We show that at the mean-field level there exist one-parameter families of such stable distributions, each distribution being characterized by its decay at infinity. We explain how the mean-field theory can be improved by taking into account the effect of pair or higher correlations. For some models one can check that the pair and higher correlations are factorized, meaning that correlations are absent and that therefore the mean-field theory is exact. Finally, we show that a very simple model of domain growth related to spinodal decomposition, the one-dimensional Potts model in the limit of an infinite number of states, also possesses a one-parameter family of stable distributions analogous to what we obtained for breath figures.

PACS number(s): 64.70.Fx, 68.45.Da, 02.50.+s, 05.20.Dd

I. INTRODUCTION

Breath figures are the patterns formed by growing and coalescing droplets when vapor condenses on a nonwetting surface. For example, one sees breath figures on a window pane on a cold day.

Laboratory experiments of breath figures may be performed by letting a gas saturated with water vapor pass over a cold surface [1–4]. The water condenses on the surface in the form of droplets, and the evolution of these droplets in time is recorded and analyzed.

One can distinguish three time regimes in an experiment.

In the beginning, droplets nucleate and start growing; they are widely spaced from one another compared to their sizes. The diameter of a droplet is found to be growing as a power law in time.

In the second regime, the droplets have grown to the extent that the distances between them are of the same order of magnitude as their sizes so that now there are many coalescence events. In such an event, two droplets merge very rapidly into a single droplet whose diameter is given by conservation of mass. The center of the new droplet is located between the centers of the two original merging droplets. In this regime the system appears to be statistically self-similar in time: the distributions of droplet sizes at different times are found to superpose after appropriate rescaling. One can also look at the coverage of the surface, that is, the fraction of the surface covered by water droplets, as a function of time. It is seen that after an initial rise of the coverage during the first regime, it attains a plateau in the second regime. This signifies that the spaces between the droplets are scaling in time with the same scaling law as the droplet diameters. Quantitatively, the constant coverages found in experiments are approximately 0.55 for a two-dimensional substrate, and 0.8 for a quasi-one-dimensional substrate [1,2]. These figures are very close to the jamming limit found in random-sequential-adsorption (RSA) processes. One-dimensional RSA (otherwise known as the "parking problem") consists in placing equally sized line segments sequentially at random places along a line without overlaps. When there is no more room left, one is at the jamming limit and the coverage of the line is calculated to be 0.748 [5,6]. A two-dimensional version would be placing equally sized disks on a plane, simulations showing a jamming limit of 0.547 [7]. Inspection of a breath figure in the scaling regime shows that it is almost jammed, that is, one could hardly fit any more droplets, even of the smallest found in the figure, in the spaces left between the droplets.

In a third regime the intervals of time between coalescences and the spaces between the droplets are large enough to allow new droplets to nucleate.

In this article we consider several simplified models of breath figures in one dimension. For all these models, the combined effects of growth and of coalescence of droplets lead to a scale-invariant regime with a stable distribution of the distances between droplets. In Sec. II we present the results of numerical simulations for the system of three-dimensional droplets growing on a one-dimensional substrate. We observe that after a transient regime, a scaling regime emerges as the coverage becomes constant and the distributions of the diameters, gaps, and distances between the droplets become invariant (up to a rescaling). In Sec. III we consider a simplified model (called the "cut-in-two" model) of growing droplets such that a configuration of the system is characterized by the distances between droplets only (all droplets are assumed to be of the same size). We propose a mean-field theory

for this simplified model which gives a result for the scale-invariant distribution of the interdroplet distances qualitatively similar to the one observed in the simulation of the model. We discuss how the result of this mean-field theory can be improved by taking into account the effect of correlations between pairs of neighboring interdroplet distances. One interesting outcome of the mean-field theory is the existence of a one-parameter family of scale-invariant distributions of interdroplet distances indexed by their power-law decay at infinity. In Sec. IV we consider another simplified one-dimensional model (called the "paste-all" model). For this model too, we develop a mean-field theory which, again, gives a one-parameter family of scale-invariant distributions. However, in this second model, one can show that the dynamics does not produce any correlation between successive interdroplet distances along the line, implying that the mean-field theory is exact, as observed in numerical simulations. The existence of a one-parameter family of scale-invariant distributions can also be observed in other problems. In the Appendix, we discuss the simple example of the growth of domains which occurs when a one-dimensional chain of Potts spins is quenched to zero temperature. Finally we conclude by adding some comments on the two-dimensional versions of the models studied in Secs. III and IV and on the possible connection of RSA with this problem.

II. SIMULATIONS OF BREATH FIGURES

In order to illustrate the existence of a scale-invariant regime in breath figures we first describe simulations of a model giving a simple description of the experiments for breath figures on a one-dimensional substrate. Such simulations have already been performed [2,3,8–10]. Here we will concentrate on the distribution of distances between the droplets. The two ingredients necessary to define a model are the growth law of the droplet sizes, and the coalescence rule, i.e., how the size and the position of the new droplet depend on those of the two coalescing droplets. The model described below will serve as a basis to yet simpler ones studied in the following sections.

(i) The law we use for the growth of a droplet diameter is [2,3,8]

$$d_i(t)=A_i t^{\mu} , \tag{1}$$

where the exponent μ relates to the condensation mechanism. Note that this law fixes a common time origin for all the droplets, the time of the beginning of the experiment. The same time origin remains after coalescences. As a consequences two droplets of the same size at different times will grow at different rates. This law is supported by experimental observations [2,3]. Another form has been proposed [9,10] for the evolution in time of the diameters, namely,

$$\frac{d}{dt}d_i(t)=B[d_i(t)]^{\omega} \tag{2}$$

which leads to a different time origin for each droplet, but to a time-invariant growth rate. In both cases, the only important ingredient is that the diameters increase with time, and therefore one expects that replacing Eq. (1) by Eq. (2) would not change any qualitative feature.

(ii) In a coalescence of two droplets of diameters d_i and d_j, mass conservation imposes that the diameter of the new droplet be given by [10,11]

$$d=(d_i^D+d_j^D)^{1/D} . \tag{3}$$

D is the dimensionality of the droplets, equal to 3 for real droplets. We will also consider D different from 3. Whenever $D>1$, Eq. (3) implies that

$$d<d_i+d_j . \tag{4}$$

Here we will locate the center of the new droplet at the center of mass of the two merging ones. One could also have located it at the center of the largest one ("majority rule"). The physical processes which occur when two droplets coalesce, in particular the movements of droplets on the substrate, are complicated. The resulting position is observed in experiments to be somewhere between the position of the largest droplet and the center of mass of the two coalescing droplets [11]. This has been analyzed in Refs. [10], and [11].

We use periodic boundary conditions to simulate this model. The quantities of interest in the system are droplet diameters d_i, distances between centers of neighboring droplets h_i (which we call intervals), and gaps between the droplets g_i. The coverage of the line is given by

$$C=\sum_i d_i \Big/ \sum_i h_i . \tag{5}$$

For convenience we denote the prefactor A of Eq. (1) as

$$A_i=w_i^{1/D} \tag{6}$$

where w_i is a weight factor. The coalescence of droplets i and $i+1$ will result in a droplet of weight $w=w_i+w_{i+1}$. Two droplets coalesce when the gap between them is filled. The gaps are given by

$$g_i=h_i-\tfrac{1}{2}(d_i+d_{i+1})=h_i\left[1-\frac{t^{\mu}}{\tau_i}\right] \tag{7}$$

with

$$\tau_i=\frac{2h_i}{w_i^{1/D}+w_{i+1}^{1/D}} \tag{8}$$

an effective coalescence time. If $\tau_k=\min_i\{\tau_i\}$ then at time $t=\tau_k^{1/\mu}$ the gap g_k will vanish, while all other gaps will still be nonzero. In this manner one does not need to take small time increments in the simulation, but can advance from one coalescence event to the next one, while keeping count of real time.

The simulations presented here concern systems of 100 000 initial droplets of equal weight with a random distribution of intervals uniformly distributed between 0 and 1. Figure 1 shows the coverage as a function of the average diameter $\bar{d}$ for droplets with $D=3$. The coverage initially rises from zero and eventually reaches a constant value of 0.79. When the plateau is attained there are about 20 000 droplets left. The average diameter at that

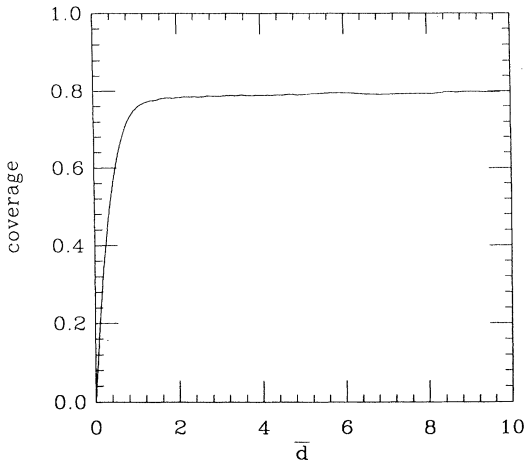

FIG. 1. Coverage as a function of the average diameter in the one-dimensional $D=3$ droplet model.

time is about the size of the largest interval at the beginning of the simulation. Its dependence in time follows a power law, as predicted by the scaling theory [10,11]. In Fig. 2 we plot distributions $p(\ )$ of lengths of intervals h, diameters d, and gaps g at five different times in the constant coverage regime, corresponding to 10 000, 9000, 8000, 7000, and 6000 droplets left. These plots have been scaled by the average diameter at each time. The plots look superposed, indicating a self-similar regime with a single length scale. Note that there is very little overlap between the distributions of gaps and diameters, i.e., almost all gaps are smaller than the smallest droplet. In other words, these are almost-jammed states. Figure 3 shows the system of droplets along the line obtained by simulation of the model, starting with 1000 droplets, for final states of 50, . . . , 10 droplets left. These results are reproduced qualitatively for different dimensionalities of

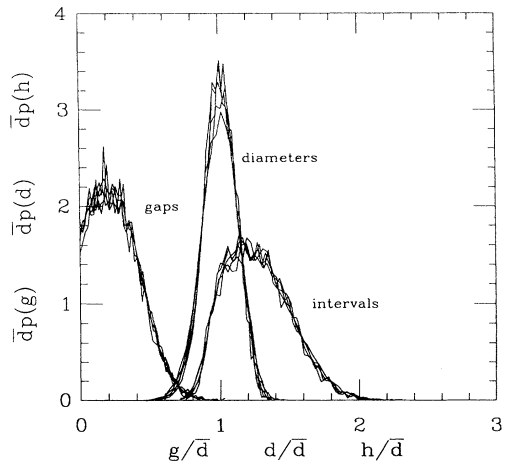

FIG. 2. Distributions of lengths of intervals, diameters, and gaps, in the one-dimensional $D=3$ droplet model, at five different times in the constant coverage regime corresponding to 10 000, 9000, 8000, 6000 droplets left.

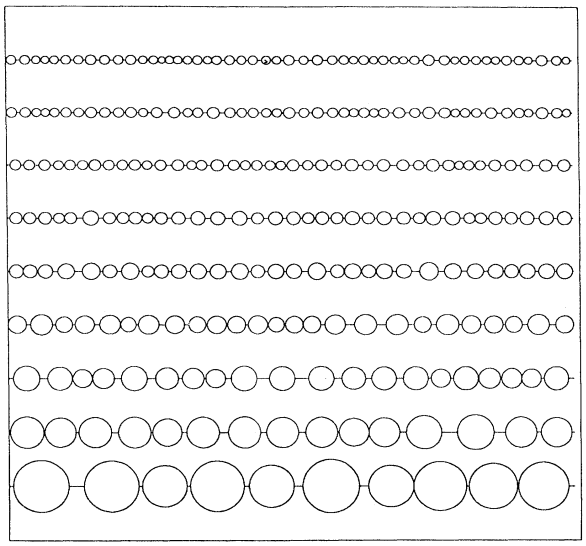

FIG. 3. Simulation of the one-dimensional $D=3$ droplet model: patterns obtained starting with 1000 droplets, for final states of 50, . . . , 10 droplets left.

droplets. The value of constant coverage in the scaling regime depends on the dimensionality of the droplets. In Fig. 4 we plot the constant coverage as a function of D. In the limit $D\rightarrow 1$ the coverage is 1 since in this case there is no contraction of the droplets in the coalescence [cf. Eq. (3)]. In the limit $D\rightarrow\infty$ one finds a coverage of 0.72. For comparison we have marked in Fig. 4 the value of the coverage in the jamming limit. One also finds that the distribution of diameters becomes narrower as D is increased which is a simple consequence of the rule for coalescence of droplets Eq. (3). In the limit $D\rightarrow\infty$, Eq. (3) becomes

$$d=\max\{d_i,d_j\}\ . \tag{9}$$

Therefore if initially one takes all droplets with the same size, this property remains true all along the evolution of

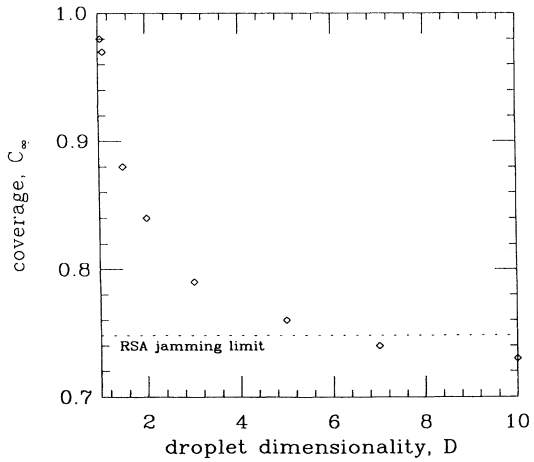

FIG. 4. Limit coverage as a function of the dimensionality D.

the system; in other terms the distribution of diameters is a δ function.

This remark leads us naturally to introduce the geometrical models of the following sections which, though much simpler, capture the essence of the model described in this section.

III. A GEOMETRICAL MODEL: THE "CUT-IN-TWO" MODEL

Consider a line with points scattered on it. At each step, one searches for the two closest points, and replaces these two points by a single point midway between them.

If we denote by h_i the interval separating the points i and $i+1$, the process can be described as searching for the shortest interval, which we denote by $\tilde{h}$, cutting it in two and pasting each half to its neighboring interval.

The connection of this simplified model with the droplet model for breath figures described in the preceding section is seen if we place equally sized droplets, each centered on one of the points on the line, and allow the droplets to grow all at the same rate. When two droplets touch, at which time all the droplets are of diameter $\tilde{h}$, they coalesce into a droplet of the *same* diameter centered in the middle of the coalescing droplets. This model resembles the infinite D-dimensional droplet model very much, though they differ with respect to the locations of the centers of the droplets after coalescence.

Let us give the results of a simulation of this model. The coverage as a function of $\tilde{h}$ may be computed numerically, using Eq. (5),with $d_i=\tilde{h}$ for all i. Starting from zero, it rises up to a plateau at a value of $C=0.72$. In Fig. 5 we show the distribution of interval lengths at five different times in the constant coverage regime (same as those taken for Fig. 2), scaled by $\tilde{h}$. This simple geometric model exhibits a long time behavior similar to the droplet model of the preceding section.

A. Mean-field theory

To study this geometrical model analytically, we start with a mean-field approximation, assuming no correlations between lengths of neighboring intervals. This approach has already been presented elsewhere [12], but we describe it here for completeness.

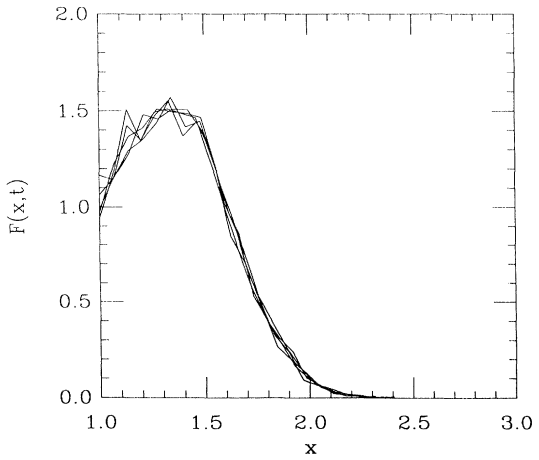

FIG. 5. Distribution of interval lengths at five different times (same as for Fig. 2) in the constant coverage regime, scaled by $\tilde{h}$, for the cut-in-two model.

To visualize this approximation, consider the following process: one has a sack with sticks of different lengths (representing the intervals). At each step one looks for the shortest stick in the sack, cuts it into two halves, and pastes them to two other sticks chosen at random from the sack.

We define $n_t(h)\delta h$ as the number of sticks of length between h and $h+\delta h$ at time t. The total number of sticks, the total length of the sticks, and the coverage are given, respectively, by

$$N_t=\int_{\tilde{h}}^{\infty} n_t(h)dh \ , \tag{10}$$

$$L=\int_{\tilde{h}}^{\infty} h n_t(h)dh \ , \tag{11}$$

$$C_t=\tilde{h}N_t/L \ . \tag{12}$$

We can describe the evolution of $n_t(h)$ by a Smoluchovski equation [13]. During a time increment δt we coalesce all sticks of length between $\tilde{h}$ and $\tilde{h}+\delta\tilde{h}$. Using the fact that the probability of finding a stick of length h is $n_t(h)\delta h/N_t$ we can write

$$n_{t+\delta t}(h)=n_t(h)+\frac{2n_t(\tilde{h})\delta\tilde{h}}{N_t}[-n_t(h) +n_t(h-\tfrac{1}{2}\tilde{h})\Theta(h-\tfrac{3}{2}\tilde{h})] \tag{13}$$

the factor 2 arising since there are two sticks involved in each coalescence (apart from $\tilde{h}$). The first term inside the square brackets corresponds to sticks of length h becoming sticks of length $h+\tilde{h}/2$ under coalescence, the second to sticks of length $h-\tilde{h}/2$ becoming sticks of length h. The total number of sticks remaining is

$$N_{t+\delta t}=N_t-n_t(\tilde{h})\delta\tilde{h} \ . \tag{14}$$

We next define $f_t(h)\delta h$ as the fraction of sticks of lengths between h and $h+\delta h$,

$$f_t(h)=n_t(h)/N_t \tag{15}$$

which obeys, to first order in $\delta\tilde{h}$, the equation

$$f_{t+\delta t}(h)=f_t(h)+[-f_t(h)+2f_t(h-\tfrac{1}{2}\tilde{h})\Theta(h-\tfrac{3}{2}\tilde{h})] \times f_t(\tilde{h})\delta\tilde{h} \ . \tag{16}$$

As $\tilde{h}$ is the natural length scale in the problem it is convenient to define a scaled distribution $F(x,t)$ with support $(1,\infty)$ by

$$f_t(h)=\tilde{h}^{-1}F(h/\tilde{h},t) \tag{17}$$

for which we find in the limits $\delta t\to 0$, $\delta\tilde{h}\to 0$ a nonlinear partial differential equation

$$\gamma(t)\frac{\partial F(x,t)}{\partial t}=F(x,t)+x\frac{\partial F(x,t)}{\partial x} +F(1,t)[2F(x-\tfrac{1}{2},t)\Theta(x-\tfrac{3}{2})-F(x,t)] \tag{18}$$

where $\gamma(t)=\tilde{h}(d\tilde{h}/dt)^{-1}$ relates the minimal length $\tilde{h}$ with the physical time t. Since this relation is arbitrary in this model, we set $\gamma(t)=1$. To solve Eq. (18) we introduce the Laplace transform of $F(x,t)$

$$\phi(p,t)=\int_1^\infty dx\,\exp(-px)F(x,t) \tag{19}$$

which obeys the equations

$$\frac{\partial\phi(p,t)}{\partial t}=-p\frac{\partial\phi(p,t)}{\partial p}+F(1,t)[2\exp(-p/2)-1]\phi(p,t)-F(1,t)\exp(-p)\ . \tag{20}$$

While we could not solve the complete time evolution of this equation, its stationary solutions [i.e., with the left-hand side of Eq. (20) equal to 0 and $F(1,t)=F(1)$] are easily calculated. There exists a continuum of such solutions, each characterized by a parameter $F(1)$,

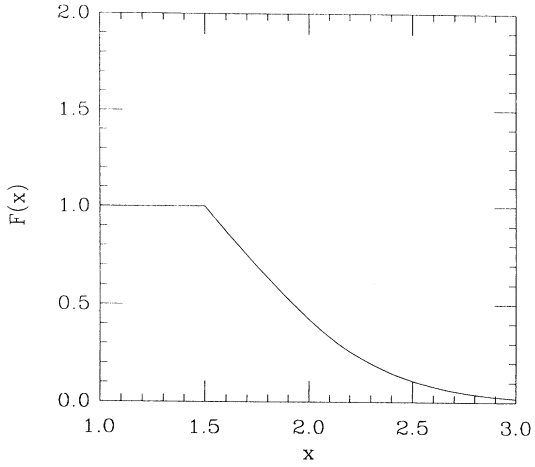

FIG. 6. Scaled distribution of interval lengths $F(x,t)$ in the mean-field theory, for the cut-in-two model.

$$\phi(p)=F(1)\int_p^\infty dt\frac{1}{t}\exp\left[-t+F(1)\int_p^t du\frac{1-2\exp(-u/2)}{u}\right]\ . \tag{21}$$

The unsolved question is to know which stationary solution (if any) is selected by a given initial condition. Let us note that Eq. (21) is obtained from Eq. (20) by considering that $\phi(p)$ and $F(1)$ are independent quantities. In fact, from the definition of $\phi(p)$, Eq. (19), they are related by a consistency relation:

$$\lim_{p\to\infty} pe^p\phi(p)=F(1)\ . \tag{22}$$

It is easy to check that $\phi(p)$ in Eq. (21) does satisfy this relation. The coverage in this asymptotic regime is given by $C_\infty=1/\bar{x}=-1/\phi'(0)$. Expanding Eq. (21) for small p,

$$1-\phi(p)\sim p^{F(1)}\ , \tag{23}$$

we see that the only solution producing a finite nonzero value of the coverage is given by the choice $F(1)=1$. This is in fact the asymptotic value for the scaled distribution found either by simulations of the model, or by iterating Eq. (16), for most initial distributions. In our previous work [12] we gave an argument based on the motion of the singularities in the complex plane of $\phi(p)$ to explain why the system converges to the solution with $F(1)=1$: if $\phi(p,0)$ is analytic in the neighborhood of $p=0$, the singularities go to infinity. Other stationary solutions with $F(1)<1$ are nevertheless possible for some more special initial conditions. Finally the case $F(1)>1$ is ruled out since it would correspond to distributions such that $\bar{x}=0$. For $F(1)=1$ we calculated a coverage of 0.646. In Fig. 6 we plot the scaled distribution of lengths $F(x,t)$ in the long time limit of the recurrence relation (16). Comparing Figs. 5 and 6, it is clear that the mean-field approach is not accurate enough for a quantitative understanding of this model.

B. Role of correlations

An exact treatment of the model needs to take into account the correlations between interval lengths, which may be done as follows. If we denote by $f_t^{(k)}(h_1,h_2,\ldots,h_k)$ the probability of finding a k-tuple of successive intervals of lengths $h_1,\ldots,h_k$ at time t, we can write a hierarchy of recursion relations for the evolution in time of these probabilities, assuming that the coalescences occur one at a time. In a small time step δt, during which $\tilde{h}$ is changed by $\delta\tilde{h}$, the first two equations read

$$f_{t+\delta t}^{(1)}(h_1)[1-f_t^{(1)}(\tilde{h})\delta\tilde{h}]=f_t^{(1)}(h_1)-[f_t^{(2)}(\tilde{h},h_1)+f_t^{(2)}(h_1,\tilde{h})]\delta\tilde{h}+\left[f_t^{(2)}\left[\tilde{h},h_1-\frac{\tilde{h}}{2}\right]+f_t^{(2)}\left[h_1-\frac{\tilde{h}}{2},\tilde{h}\right]\right]\Theta(h_1-\tfrac{3}{2}\tilde{h})\delta\tilde{h}\ , \tag{24}$$

$$f_{t+\delta t}^{(2)}(h_1,h_2)[1-f_t^{(1)}(\tilde{h})\delta\tilde{h}]=f_t^{(2)}(h_1,h_2)-[f_t^{(3)}(\tilde{h},h_1,h_2)+f_t^{(3)}(h_1,h_2,\tilde{h})]\delta\tilde{h}+f_t^{(3)}\left[\tilde{h},h_1-\frac{\tilde{h}}{2},h_2\right]\Theta(h_1-\tfrac{3}{2}\tilde{h})\delta\tilde{h}+f_t^{(3)}\left[h_1,h_2-\frac{\tilde{h}}{2},\tilde{h}\right]\Theta(h_2-\tfrac{3}{2}\tilde{h})\delta\tilde{h}+f_t^{(3)}\left[h_1-\frac{\tilde{h}}{2},\tilde{h},h_2-\frac{\tilde{h}}{2}\right]\Theta(h_1-\tfrac{3}{2}\tilde{h})\Theta(h_2-\tfrac{3}{2}\tilde{h})\delta\tilde{h}\ . \tag{25}$$

Unfortunately this infinite hierarchy of equations is intractable. Nevertheless it is possible to consider successive approximations to them. For instance, the mean-field theory approximation Eq. (16) described above consists in considering the intervals as independent, which implies that the probability $f_t^{(2)}(h_1,h_2)$ factorizes into the product $f_t^{(1)}(h_1)f_t^{(1)}(h_2)$ in the first equation. The next step consists in taking into account correlations between nearest neighbors only. This is done by means of a decomposition of sequence of intervals into overlapping independent pairs:

$$\begin{array}{c} \ldots,h_1,h_2,h_3,h_4,\ldots \\ \downarrow \\ \ldots,(h_1,h_2),(h_2,h_3),(h_3,h_4),\ldots \end{array} \quad (26)$$

A coalescence event where the three intervals $h_1,\tilde{h},h_2$ transform into the two intervals $h_1+\tilde{h}/2$, $h_2+\tilde{h}/2$ will be described by the transformation of four pairs into three

$$\begin{array}{c} (h_3,h_1),(h_1,\tilde{h}),(\tilde{h},h_2),(h_2,h_4) \\ \downarrow \\ (h_3,h_1+\tfrac{1}{2}\tilde{h}),(h_1+\tfrac{1}{2}\tilde{h},h_2+\tfrac{1}{2}\tilde{h}),(h_2+\tfrac{1}{2}\tilde{h},h_4)\ . \end{array} \quad (27)$$

The probability of finding a sequence of three intervals h_1,h_2,h_3 is given, in this approximation of independent pairs, by

$$f_t^{(3)}(h_1,h_2,h_3)=\frac{f_t^{(2)}(h_1,h_2)f_t^{(2)}(h_2,h_3)}{f_t^{(1)}(h_2)}\ . \quad (28)$$

Equation (25) becomes

$$\begin{aligned} f_{t+\delta t}^{(2)}(h_1,h_2)[1-f_t^{(1)}(\tilde{h})\delta\tilde{h}] &= f_t^{(2)}(h_1,h_2)-f_t^{(2)}(h_1,h_2)\left[\frac{f_t^{(2)}(\tilde{h},h_1)}{f_t^{(1)}(h_1)}+\frac{f_t^{(2)}(h_2,\tilde{h})}{f_t^{(1)}(h_2)}\right]\delta\tilde{h} \\ &+\frac{f_t^{(2)}(\tilde{h},h_1-\frac{1}{2}\tilde{h})f_t^{(2)}(h_1-\frac{1}{2}\tilde{h},h_2)}{f_t^{(1)}(h_1-\frac{1}{2}\tilde{h})}\Theta(h_1-\tfrac{3}{2}\tilde{h})\delta\tilde{h} \\ &+\frac{f_t^{(2)}(h_1,h_2-\frac{1}{2}\tilde{h})f_t^{(2)}(h_2-\frac{1}{2}\tilde{h},\tilde{h})}{f_t^{(1)}(h_2-\frac{1}{2}\tilde{h})}\Theta(h_2-\tfrac{3}{2}\tilde{h})\delta\tilde{h} \\ &+\frac{f_t^{(2)}(h_1-\frac{1}{2}\tilde{h},\tilde{h})f_t^{(2)}(\tilde{h},h_2-\frac{1}{2}\tilde{h})}{f_t^{(1)}(\tilde{h})}\Theta(h_1-\tfrac{3}{2}\tilde{h})\Theta(h_2-\tfrac{3}{2}\tilde{h})\delta\tilde{h}\ . \end{aligned} \quad (29)$$

We also define scaled probability densities $G(x,y,t)$ and $F(x,t)$ by

$$f_t^{(2)}(h_1,h_2)=\tilde{h}^{-2}G(h_1/\tilde{h},h_2/\tilde{h},t)\ , \quad (30)$$

$$f_t^{(1)}(h)=\tilde{h}^{-1}F(h/\tilde{h},t)\ . \quad (31)$$

The recurrence relation (29)—for which we did not find any analytical treatment—has been iterated in time. Again, after a sharp rise, the coverage settles off at a constant value of 0.69. In Fig. 7 we plot $F(x,t)$ obtained by iterating Eq. (29). Comparing this to Fig. 6 we see that this is a better approximation than the mean-field approximation, particularly in the fact that most of the weight of the distribution is between 1 and 2, signifying an almost-jammed state.

Nevertheless, this approximation, restricted to considering correlations between nearest neighbors, has only limited accuracy since it does not reproduce the full shape of $F(x,t)$ found in Fig. 5, which implies that the model exhibits more complex correlations. When one cuts the interval $\tilde{h}$ into two halves and pastes each of them to its neighbor, one creates a correlation between the lengths of the two resulting intervals. This may be checked by plotting (Fig. 8) the scaled correlation function γ_k for lengths of neighboring intervals, defined by

$$\gamma_k=\tilde{h}^{-2}(\overline{h_i h_{i+k}}-\bar{h}_i^{\,2})\ . \quad (32)$$

Since correlations decay rapidly with k one expects that higher-order approximations would lead to an improved $F(x,t)$, with a rapid convergence rate.

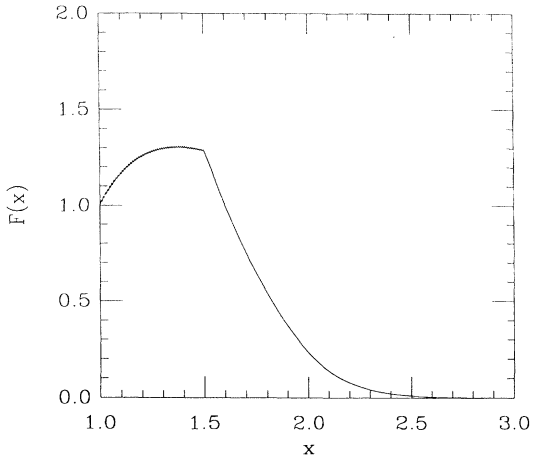

FIG. 7. Scaled distribution of interval lengths $F(x,t)$ in the pair correlation approximation, for the cut-in-two model.

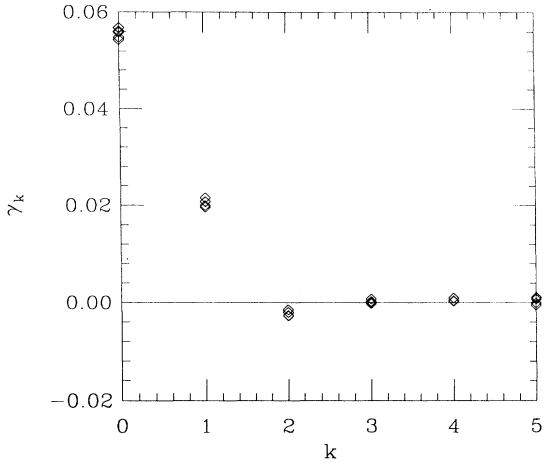

FIG. 8. Scaled correlation function γ_k for lengths of neighboring intervals, for the cut-in-two model.

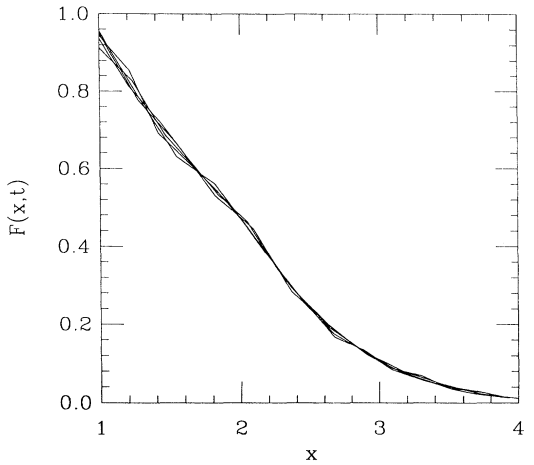

FIG. 9. Scaled distribution of interval lengths $F(x,t)$ for the paste-all model at five different times (same as for Fig. 2) in the scaling regime.

IV. A SIMPLER GEOMETRICAL MODEL: THE "PASTE-ALL" MODEL

Let us introduce a variant of the previous model. Again we start with randomly distributed intervals on the line. At each step one searches for the shortest interval which is now pasted as a whole to either one of its neighbors, with equal probability. Here too we look at the long time behavior of the system. A simulation of the model shows that the coverage of the line as a function of $\tilde{h}$ attains a constant value of $C \approx 0.56$ after a transient period. In Fig. 9 we show the scaled distribution of interval lengths $F(x,t)$ at five different times in the scaling regime. The interest in this model becomes apparent when one looks at the scaled correlation function for lengths of neighboring intervals γ_k defined in Eq. (32). In Fig. 10 we plot γ_k at different times in the scaling regime. It is seen that there are no correlations between lengths of neighboring intervals, which indicates that a mean-field description should be exact.

This is in fact the case as will be shown now. Consider the first two equations of the hierarchy of recursion relations for the probabilities $f_t^{(k)}(h_1,h_2,\ldots,h_k)$ defined as above:

$$f_{t+\delta t}^{(1)}(h_1)[1-f_t^{(1)}(\tilde{h})\delta\tilde{h}]=f_t^{(1)}(h_1)-\tfrac{1}{2}[f_t^{(2)}(\tilde{h},h_1)+f_t^{(2)}(h_1,\tilde{h})]\delta\tilde{h}$$
$$+\tfrac{1}{2}[f_t^{(2)}(\tilde{h},h_1-\tilde{h})+f_t^{(2)}(h_1-\tilde{h},\tilde{h})]\Theta(h_1-2\tilde{h})\delta\tilde{h}\ , \tag{33}$$

$$f_{t+\delta t}^{(2)}(h_1,h_2)[1-f_t^{(1)}(\tilde{h})\delta\tilde{h})]=f_t^{(2)}(h_1,h_2)-\tfrac{1}{2}[f_t^{(3)}(\tilde{h},h_1,h_2)+f_t^{(3)}(h_1,h_2,\tilde{h})]\delta\tilde{h}$$
$$+\tfrac{1}{2}[f_t^{(3)}(\tilde{h},h_1-\tilde{h},h_2)+f_t^{(3)}(h_1-\tilde{h},\tilde{h},h_2)]\Theta(h_1-2\tilde{h})\delta\tilde{h}$$
$$+\tfrac{1}{2}[f_t^{(3)}(h_1,\tilde{h},h_2-\tilde{h})+f_t^{(3)}(h_1,h_2-\tilde{h},\tilde{h})]\Theta(h_2-2\tilde{h})\delta\tilde{h}\ . \tag{34}$$

It can now be seen that these probabilities factorize, that is, taking the form

$$f_t^{(k)}(h_1,\ldots,h_k)=f_t(h_1)f_t(h_2)\cdots f_t(h_k) \tag{35}$$

is consistent with each of the recurrence relations, to first order in $\delta\tilde{h}$. Therefore it is sufficient to regard the relation

$$f_{t+\delta t}^1(h)=f_t^1(h)+f_t^1(\tilde{h})f_t^1(h-\tilde{h})\delta\tilde{h}\Theta(h-2\tilde{h}) \tag{36}$$

which is found by the factorization of Eq. (33). Figure 11 shows the scaled distribution of intervals in the long time limit of iteration of Eq. (36), matching very well the distributions in Fig. 9.

The scaled probability distribution $F(x,t)$ obeys the partial differential equation

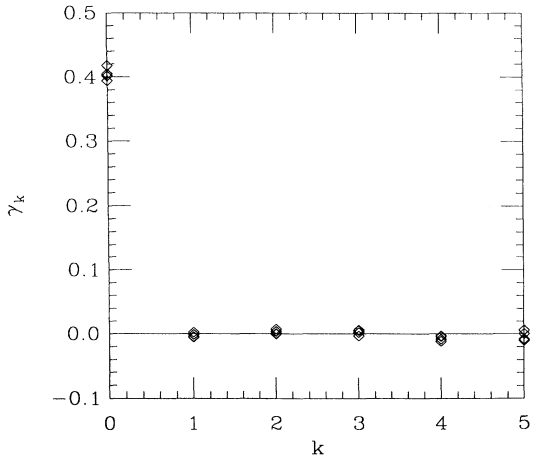

FIG. 10. Scaled correlation function γ_k for the paste-all model.

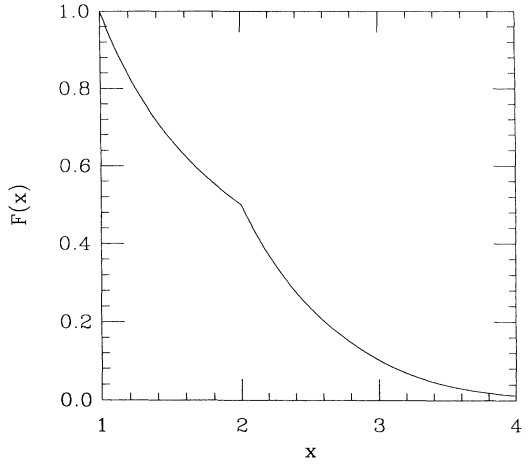

FIG. 11. Scaled distribution of interval lengths $F(x,t)$ for the paste-all model in the mean-field approximation.

$$\frac{\partial F(x,t)}{\partial t}=F(x,t)+x\frac{\partial F(x,t)}{\partial x}+F(1,t)F(x-1,t)\Theta(x-2) \tag{37}$$

[having set $\gamma(t)=1$] which reads, in Laplace space,

$$\frac{\partial \phi(p,t)}{\partial t}=-p\frac{\partial \phi(p,t)}{\partial p}+F(1,t)e^{-p}[\phi(p,t)-1]\ . \tag{38}$$

The stationary solutions of Eq. (38) are

$$\phi(p)=1-\exp\left[-F(1)\int_p^\infty \frac{e^{-u}}{u}du\right]$$
$$=1-\exp[-F(1)\mathrm{Ei}(p)] \tag{39}$$

where $\mathrm{Ei}(p)$ is the exponential integral function. Arguing as before, only the solution with $F(1)=1$ corresponds to a distribution with a finite average, and therefore a finite coverage. The coverage C_∞ may be computed by expanding $\mathrm{Ei}(p)$ around $p=0$:

$$\mathrm{Ei}(p)\simeq -\gamma-\ln p \tag{40}$$

where $\gamma\approx 0.577$ is the Euler constant. Hence $\bar{x}=e^{\gamma}\approx 1.78$, implying that $C_\infty\approx 0.56$.

As mentioned in the preceding section, solutions with $F(1)>1$ are unacceptable since they give $\bar{x}=0$ which would correspond to stationary solutions with negative parts.

There remains the question of solutions with $F(1)<1$. For this class of solutions, $\bar{x}=-\phi'(0)\to\infty$ which means these are slowly decaying distributions. In Fig. 12 we plot stationary solutions of Eq. (37) obtained by integrating the equation with $F(1)=0.5,0.9,0.99,1$. One sees that indeed for $F(1)<1$ the distributions display power-law decay, $F(x)\simeq x^{-[1+F(1)]}$, while for $F(1)=1$ the decay is much faster. Let us consider the space of the distributions on the support $(1,\infty)$ with the dynamics given by Eq. (37). In this space, fixed points correspond to stationary solutions of Eq. (37) [given, alternatively, by the inverse Laplace transform of Eq. (38)]. It would be interesting to know the size of the basins of attraction of these fixed points and whether there could be trajectories other than those which converge to these attractors.

One can study the stability of these fixed points to perturbations by looking at the eigenvectors of the linear operator obtained by linearizing Eq. (38) around a given fixed point. Consider an eigenvector of the linear operator obtained by linearizing Eq. (38) around a given fixed point. Consider an eigenvector of eigenvalue λ of this linearized operator. Inserting

$$\phi(p,t)=\phi(p)+\epsilon h(p)e^{-\lambda t}\ , \tag{41}$$

$$F(1,t)=F(1)+\epsilon g e^{-\lambda t}\ , \tag{42}$$

where $\phi(p)$ is a solution of the form (39), into Eq. (38) and retaining terms of the first order in ϵ, we find a differential equation for $h(p)$,

$$ph'(p)=[\lambda+F(1)e^{-p}]h(p)+ge^{-p}[\phi(p)-1]\ . \tag{43}$$

The solution of Eq. (43), under the constraint

$$\lim_{p\to\infty} pe^{p}h(p)=g \tag{44}$$

coming from the definition of the Laplace transform, is

$$h_\lambda(p)=g\exp\left[-F(1)\int_p^\infty \frac{e^{-u}}{u}du\right]\int_1^\infty \frac{e^{-ps}}{s^{1+\lambda}}ds\ . \tag{45}$$

Due to the normalization of $F(x)$ we have

$$h(0)=0 \tag{46}$$

implying that $\lambda>-F(1)$. For $p\ll 1$ we find that $h_\lambda(p)$ behaves as

$$h(p)\simeq \begin{cases} p^{F(1)}, & \lambda>0 \text{ (stable)} \\ p^{\lambda+F(1)}, & -F(1)<\lambda<0 \text{ (unstable)}\ . \end{cases} \tag{47}$$

Since the behavior of $h(p)$ for $p\ll 1$ is related to the decay of the distribution for large x, this linear analysis around the fixed points shows that a given solution is unstable when adding to it perturbations which decrease

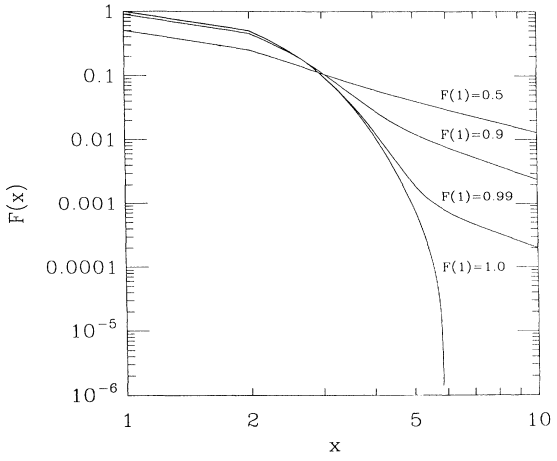

FIG. 12. Stationary solutions obtained by integrating Eq. (37) with $F(1)=0.5,0.9,0.99,1$.

more slowly at infinity. We have not been able to solve the more general problem of the determination of the stationary solution towards which the evolution Eq. (38) converges for a given initial condition. Even generating numerically initial conditions that converge towards other stationary solutions than that given by $F(1)=1$ is not easy (when one starts with slowly decaying initial conditions, the evolution is so slow that we could never reach a stationary solution). Nevertheless we think that there should exist such initial conditions (other than starting with the stationary solution itself). In order to illustrate this possibility we treat in the Appendix a simple model for domain growth which also possesses a one-parameter family of stationary solutions. In this example one may explicitly show that the limiting stationary solution is determined by the tail of the initial distribution.

V. CONCLUSION

In this paper we have considered several simplified models for the problem of breath figures on a one-dimensional substrate. We have written and solved mean-field equations for these simplified models, which are analogous to Smoluchovski equations. These mean-field equations possess one-parameter families of scale-invariant solutions, each distribution being characterized by its decay at infinity. The solutions of these equations are exact for some cases (Sec. IV) whereas they are only approximate for the case discussed in Sec. III. We explained how to systematically improve the mean-field approximation.

The situation found in this problem is reminiscent of that encountered in the central limit theorem: the normal law is stable in the sense that the sum of many independent random variables with a common distribution gives—for most initial distributions—a normal (Gaussian) law after an appropriate rescaling. If the initial distribution is slowly decaying (as a power law) the addition of independent random variables leads to Lévy laws [14,15], i.e., to a one-parameter family of distributions described by a characteristic exponent. Here the distributions are stable in an analogous sense, which generalizes the previous one. The addition of random variables is replaced by the dynamics described in the preceding sections. The one-parameter family of scaled distributions is very similar to Lévy distributions, $F(1)$ playing here the role of the characteristic exponent of Lévy laws. In particular the case where $F(1)=1$, yielding the largest basin of attraction in the present problem, corresponds to the Gaussian, which has the largest basin of attraction for the problem of the addition of random variables.

The existence of such families of distributions is probably a much more general phenomenon, since it occurs also in several growth problems (cf. the Appendix and Refs. [16] and [17]). Moreover, the evolution of the distribution of distances is governed by nonlinear equations [Eqs. (18), and (37)] very similar to those which appear in problems of spinoidal decomposition [18].

The case of two-dimensional breath figures may be treated in the same way. We have computed the scaling distributions of interdroplet distances numerically, for the cut-in-two model or for the paste-all one. In both cases one finds a scale-invariant curve with a shape similar to that found in the one-dimensional case or for the problem studied in the Appendix.

Finally some comments concerning the link between the RSA problem and breath figures are in order. The patterns found in breath figures look almost jammed and therefore resemble those of the RSA problem. Also the values of the coverages are very close in both problems. However, the distributions of interdroplet distances (in the case of breath figures) or of interbond distances (in the case of the RSA problem) are different [12]. Moreover, in the case of breath figures the system is driven to a scale-invariant regime with no counterpart in the RSA problem.

ACKNOWLEDGMENTS

We thank D. Beysens, H. Flyvbjerg, P. Guénoun, and A. Steyer for useful discussions.

APPENDIX

In this appendix we give the solution of an extremely simple model of domain growth: a Potts model in one dimension at zero temperature. The problem of domain growth following a "quench" of a system of spins below its transition temperature has incited numerous theoretical works in the last few years. Quite a good understanding has been achieved for continuous theories in arbitrary dimension [19–23], but there still exist very few exactly soluble cases [18,24]. In one dimension Bray [25] has been able to calculate the pair correlation function for an Ising chain at zero temperature. He found an exact asymptotic form valid in the limits of long time and large distance.

Another exactly soluble case, even more simple, is the Potts model in one dimension in the limit of an infinite number of states. The infinite state Potts model has been used for studying the formation of polycrystalline aggregates [26] and the dynamics of soap froth [27,28].

In one dimension, for a large system and in the limit of long time, the dynamics of the Potts model at zero temperature can be treated as the diffusion of domain walls (as the walls are points) [29]. These walls diffuse and when two walls meet (signifying the elimination of a domain) one of two possibilities occurs: (i) if the two domains neighboring the disappearing domain are of the same state, the two walls are annihilated and the two domains merge into one; or (ii) if the two domains neighboring the disappearing domain are of different states, the two walls are replaced by a single diffusing wall between the two domains.

In the case of the Ising model (two states), only the first possibility occurs. In the infinite Potts model case, which we consider, it suffices to look at the evolution of a single domain bounded by two walls performing independent random walks [30]. If the two walls meet, the domain is eliminated, so we are interested only in the case that they do not meet. It is well known that the probability $p(z,y,t)$ of finding the two random walkers (which never meet between time 0 and t) at a distance z at time t, starting at a distance y is

$$p(z,y,t)=\frac{\exp[-(z-y)^2/4t]-\exp[-(z+y)^2/4t]}{\sqrt{4\pi t}} \tag{A1}$$

when the diffusion constant of each walker is 1.

Following a quench of the spin system from a high temperature to zero temperature there is a density of sizes of domains, which we shall denote by $\rho(y,0)$. This means that at time $t=0$ there are $L\rho(y,0)$ domains of size y in a sample of length L. Given this density at time $t=0$, the density of domains of length z at a later time t is given by

$$\rho(z,t)=\int_0^\infty dy\,\rho(y,0)p(z,y,t) \tag{A2a}$$

$$=\frac{\exp(-z^2/4t)}{\sqrt{4\pi t}}\int_0^\infty dy\,\rho(y,0)\exp(-y^2/4t)\times 2\sinh(zy/2t) \tag{A2b}$$

with z positive. The total number of domains decreases with time. For the asymptotic form of $\rho(z,t)$ in the long time limit, as its evolution is governed by a diffusion process, we are interested in z of the order of $\sqrt{t}$. We first consider the case of an initial density with a finite first moment at time $t=0$. In this case we can develop the integrand of Eq. (A2b) to first order in $y/\sqrt{t}$ to find

$$\rho(z,t)\cong\frac{z\exp(-z^2/4t)}{2\sqrt{\pi}t^{3/2}}\int_0^\infty dy\,\rho(y,0)y\ . \tag{A3}$$

Integrating Eq. (A3) over z we have

$$\int_0^\infty dz\,\rho(z,t)\cong\frac{1}{\sqrt{\pi t}}\int_0^\infty dy\,\rho(y,0)y \tag{A4}$$

from which we conclude that the number of domains diminishes as $t^{-1/2}$. Let us define a scaled distribution function $F(x,t)$, normalized to 1, by

$$F(x,t)dx=\left[\int_0^\infty dz'\rho(z',t)\right]^{-1}\rho(z,t)dz \tag{A5}$$

with $x=z/\sqrt{2t}$, thus obtaining

$$F(x,t)=x\exp(-x^2/2)\ , \tag{A6}$$

which is time independent [30].

Let us compare this result with a simulation of this model. Starting with 10 000 domains on a line with cyclic boundary conditions, with sizes chosen at random from a uniform distribution between 1 and 50, we let the boundary walls perform random walks in parallel. Shown in Fig. 13 are the distributions of domain sizes at four different times (when there are 5000, 4500, 4000, and 3000 domains left) scaled by the average domain size (in diamonds) and Eq. (A6) (solid line, scaled by $\bar{x}$), showing good agreement.

We next consider the case of a slowly decaying initial density such that its first moment is divergent. We assume that for $y\gg 1$

$$\rho(y,0)\cong\frac{A}{y^{1+\alpha}} \tag{A7}$$

with $0<\alpha<1$. Performing a change of variables in the integral in Eq. (A2b), $u=y/\sqrt{2t}$, we see that only the asymptotic form (A7) of $\rho(y,0)$ is important and one obtains

$$\rho(x,t)\cong\frac{A\exp(-z^2/4t)}{\sqrt{2\pi}(2t)^{(1+\alpha)/2}}\times\int_0^\infty du\frac{\exp(-u^2/2)2\sinh(zu/\sqrt{2}t)}{u^{1+\alpha}}\ . \tag{A8}$$

Integrating over z one finds that the number of domains decreases as $t^{-\alpha/2}$. As $0<\alpha<1$, the decrease is slower than in the first case. Using Eq. (A5) we calculate the scaled normalized distribution for this case

$$F(x,t)=C\exp(-x^2/2)\int_0^\infty du\frac{\exp(-u^2/2)2\sinh(xu)}{u^{1+\alpha}} \tag{A9}$$

where C is a normalization constant. Again we find that $F(x,t)$ is time independent. For $x\gg 1$, $2\sinh(xu)$

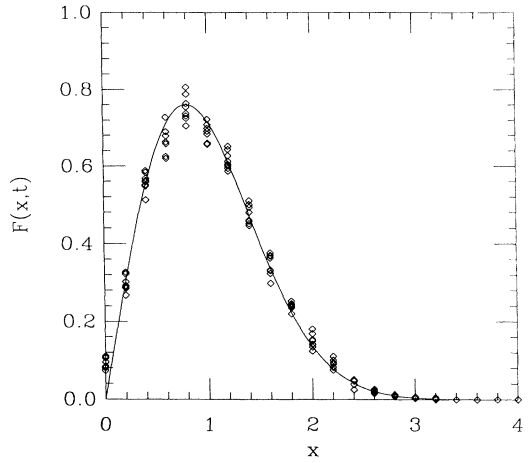

FIG. 13. Stationary distribution for the one-dimensional Potts model with a bounded initial distribution of domains (see text).

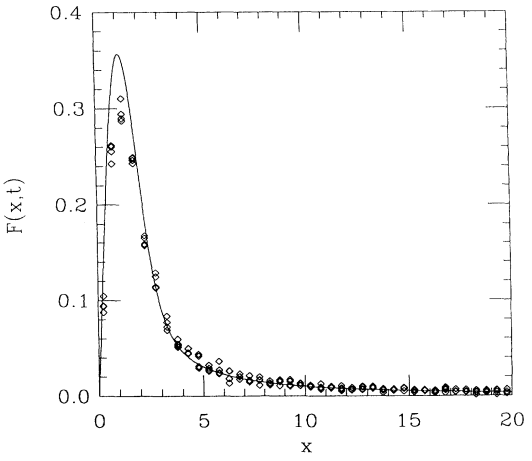

FIG. 14. Stationary distribution for the one-dimensional Potts model with a slowly decaying initial distribution of domains (see text).

$\cong \exp(xu)$ and one can see that $F(x,t)$ decays as $x^{-(1+\alpha)}$.

In Fig. 14 we show the domain size distributions found from a simulation, this time with a slowly decreasing initial distribution of sizes with an exponent $\alpha=0.5$. The distributions (in diamonds) are scaled by $\sqrt{2t}$ and compared with Eq. (A9) (solid line), again in good agreement. This example is thus an exactly soluble model which is driven in the long time limit to stationary scaling distributions. There is a whole family of such stationary solutions, indexed by the exponent α. The solution towards which the system is driven is selected by the initial conditions, specifically by the tail of the distribution. If the initial distribution decays quickly enough, such that its first moment is finite, it converges to the solution (A6), which exhibits Gaussian decay. This solution is the analog of the solutions with $F(1)=1$ in the preceding sections. If, on the other hand, the initial distribution decays slowly, namely, as a power law, we have seen that it converges to a different stationary solution, (A9), which decays at the same rate as the initial distribution. This is the analog of solutions with $0<F(1)<1$ of the preceding sections.

Lastly, let us remark that since the limiting distribution can be found by considering only a single domain, one expects that here, as in Sec. IV, a mean-field theory would give the exact scale-invariant distribution of domains.

[1] D. Beysens and C. M. Knobler, Phys. Rev. Lett. **57**, 1433 (1986), and references to earlier works therein.

[2] A. Steyer, P. Guenoun, D. Beysens, D. Fritter, and C. M. Knobler, Europhys. Lett. **12**, 211 (1990).

[3] D. Fritter, Ph.D. thesis, University of California, Los Angeles, 1989.

[4] B. J. Briscoe, and K. P. Galvin, J. Phys D **23**, 422 (1990).

[5] A. Rényi, Publ. Math. Inst. Hung. Acad. Sci. **3**, 109 (1958).

[6] B. Widom, J. Chem. Phys. **44**, 3888 (1966).

[7] R. Swendsen, Phys. Rev. A **24**, 504 (1981), and other references therein.

[8] D. Fritter, C. M. Knobler, D. Roux, and D. Beysens, J. Stat. Phys. **52**, 1447 (1988).

[9] P. Meakin and F. Family, J. Phys. A **22**, 225 (1989).

[10] F. Family, and P. Meakin, Phys. Rev. Lett. **61**, 428 (1988); Phys. Rev. A **40**, 3836 (1989).

[11] J. L. Viovy, D. Beysens, and C. M. Knobler, Phys. Rev. A **37**, 4965 (1988).

[12] B. Derrida, C. Godrèche, and I. Yekutieli, Europhys. Lett. **12**, 385 (1990).

[13] N. G. Van Kampen, *Stochastic Processes in Physics and Chemistry* (North-Holland, Amsterdam, 1981).

[14] P. Lévy, *Théorie de l'addition des variables aléatoires* (Gauthier-Villars, Paris, 1954).

[15] B. V. Gnedenko, and A. N. Kolmogorov, *Limit Distributions for Sums of Independent Random Variables* (Addison-Wesley, Reading, MA, 1954).

[16] A. J. Bray, K. Humayun, and T. J. Newman, Phys. Rev. B **43**, 3699 (1991).

[17] K. Humayun, and A. J. Bray, J. Phys. A **24**, 1915 (1991).

[18] A. Coniglio, and M. Zanetti, Europhys. Lett. **10**, 575 (1989).

[19] J. Langer, in *Solids far from Equilibrium,* edited by C. Godrèche (Cambridge University Press, Cambridge, England, 1991), Chap. 3.

[20] A. J. Bray, Phys. Rev. B **41**, 6724 (1990).

[21] O. G. Mouritsen, and J. P. Shah, Phys. Rev. B **40**, 11 445 (1989).

[22] O. G. Mouritsen, in *Kinetics of Ordering and Growth at Surfaces,* edited by M. G. Lagally (Plenum, New York, in press).

[23] J. P. Shah and O. G. Mouritsen, Phys. Rev. B **41**, 7003 (1990).

[24] D. Kandel and E. Domany, J. Stat. Phys. **58**, 685 (1990).

[25] A. J. Bray, J. Phys. A **23**, L67 (1990).

[26] M. P. Anderson, D. J. Srolovitz, G. S. Grest, and P. S. Sahni, Acta Metall. **32**, 783 (1984).

[27] C. S. Smith, in *Metal Interfaces,* edited by C. Herring (American Society for Metals, Metals Park, OH, 1952), p. 65.

[28] H. Flyvbjerg, and C. Jeppesen, Phys. Scr. **T38**, 49 (1991).

[29] The same system has been studied independently by H. Flyvbjerg (private communication).

[30] D. Ben Avraham, M. A. Burschka, and C. R. Doering, J. Stat. Phys. **60**, 695 (1990).